Fast accurate iterative reconstruction for low-statistics positron volume imaging

Phys. Med. Biol. **43** (1998) 835–846. Printed in the UK PII: S0031-9155(98)90638-8

Fast accurate iterative reconstruction for low-statistics positron volume imaging

A J Reader, K Erlandsson, M A Flower and R J Ott

Joint Department of Physics, Institute of Cancer Research, Royal Marsden NHS Trust, Downs Road, Sutton, Surrey SM2 5PT, UK

Received 31 July 1997

Abstract. A fast accurate iterative reconstruction (FAIR) method suitable for low-statistics positron volume imaging has been developed. The method, based on the expectation maximization–maximum likelihood (EM–ML) technique, operates on list-mode data rather than histogrammed projection data and can, in just one pass through the data, generate images with the same characteristics as several ML iterations. Use of list-mode data preserves maximum sampling accuracy and implicitly ignores lines of response (LORs) in which no counts were recorded. The method is particularly suited to systems where sampling accuracy can be lost by histogramming events into coarse LOR bins, and also to sparse data situations such as fast whole-body and dynamic imaging where sampling accuracy may be compromised by storage requirements and where reconstruction time can be wasted by including LORs with no counts. The technique can be accelerated by operating on subsets of list-mode data which also allows scope for simultaneous data acquisition and iterative reconstruction. The method is compared with a standard implementation of the EM–ML technique and is shown to offer improved resolution, contrast and noise properties as a direct result of using improved spatial sampling, limited only by hardware specifications.

1. Introduction

Filtered backprojection (FBP) has been used frequently for image reconstruction in positron volume imaging (PVI). However, FBP is based on an analytic inversion of noise-free continuous projection data, which are assumed to represent true line integrals through the activity distribution. FBP offers little scope for modelling noise and consequently noisy reconstructions are obtained when insufficient events are acquired. Such situations occur in dynamic studies and also with low-sensitivity scanners. Alternative reconstruction techniques have been investigated and formulated which allow full modelling of the measurement process and take account of the noisy nature of the acquired data. Shepp and Vardi (1982) proposed the expectation maximization–maximum likelihood (EM–ML) algorithm founded on the basis of Poisson statistics which allows full incorporation of a measurement system model. However, this successful technique has been hampered by slow convergence, which for fully three-dimensional implementations on standard computer platforms can be prohibitive.

Several acceleration techniques have been proposed for 2D EM–ML which are readily adaptable to the fully three-dimensional case. Lewitt and Muehllehner (1986) improved convergence speed by incorporating an over-relaxation parameter. Tanaka (1987) used a frequency amplification method to accelerate estimation of the higher-frequency components in the image. More recently the ordered subsets EM (OSEM) method has been proposed

0031-9155/98/040835+12$19.50

by Hudson and Larkin (1994) which divides the histogrammed projection data into subsets, giving a factor speed increase proportional to the number of subsets chosen. However, this method does not necessarily converge to a ML estimate. Browne and De Pierro (1996) proposed the row-action maximum-likelihood algorithm (RAMLA) which uses as many subsets as there are projections. The algorithm has proven ML convergence, but relies on optimization of a relaxation parameter. Schmidlin *et al* (1997) proposed a high-overrelaxation parameter in combination with a data subset approach to obtain high-precision images in just eight iterations. However, this method also requires careful selection of a sequence of relaxation parameters which is dependent on the image being reconstructed.

The method proposed here, which operates on list-mode data (rather than histogrammed projection data), can produce reconstructions with the same characteristics as several EM–ML iterations in just one pass through the list-mode data by operating on subsets of the data (corresponding to a series of low-statistics frames). The use of list-mode data preserves the spatial sampling accuracy of the acquired data which, for systems that do not physically bin the acquired data into tubes of response, can allow superior resolution, contrast and noise properties. List-mode ML reconstruction is also advantageous when each coincidence event has several attributes (Barrett *et al* 1997), for example in 2D time-of-flight positron emission tomography (Parra and Barrett 1998).

2. Theory

The unknown activity distribution f is assumed to be discretized into J voxels ($j = 1 \dots J$), the intensity within each voxel f_j being the integral of activity within that voxel. There are I lines of response (LORs) ($i = 1 \dots I$), and m_i is the number of counts collected in LOR i.

The EM–ML algorithm generates a sequence of image estimates f_j^k according to

$$f_j^{k+1} = \frac{f_j^k}{\sum_{i=1}^{I} a_{ij}} \sum_{i=1}^{I} \left(\frac{m_i}{q_i^k} a_{ij} \right) \tag{1}$$

where

$$q_i^k = \sum_{j=1}^{J} a_{ij} f_j^k \tag{2}$$

is the expected count in LOR i due to the current estimate f^k and a_{ij} is the probability that an emission from voxel j will be detected in LOR i. Each new estimate monotonically increases the likelihood function as defined in Shepp and Vardi (1982).

The new FAIR algorithm is based on (1) and is given by

$$f_j^{k+1} = \frac{f_j^k}{\sum_{i=1}^{I} a_{ij}} \sum_{i=1}^{M} \left(\frac{1}{q_i^k} a_{ij} \right) \tag{3}$$

where the measured data m_i are now implicitly equal to one in the numerator of the summation, and M is the number of measured events. The measured data now consist simply of a list of M LOR definitions. The normalization factor $\sum_{i=1}^{I} a_{ij}$ must include all possible measurable LORs.

The approach of (3) is extendible to a data subsets implementation

$$f_j^{kN+n+1} = \frac{f_j^{kN+n}}{\sum_{i=1}^{I} a_{ij}} \sum_{i=\alpha_n}^{\beta_n} \left(\frac{1}{q_i^{kN+n}} a_{ij} \right) \tag{4}$$

where N is the number of data subsets ($n = 1 \ldots N$) each containing M/N LORs and successive estimates (subiterations) are now indexed according to the number of data subsets that have contributed to the image. The summation is defined over the measured list-mode data according to the following range

$$\alpha_n = \frac{(n-1)M}{N} + 1 \qquad \beta_n = \frac{nM}{N}. \tag{5}$$

3. Implementation

3.1. Detector geometry

FAIR and the standard EM–ML algorithm were implemented using the geometry of a rotating planar detector (RPD) PVI scanner, and the system transfer matrix (a_{ij}) was modelled by the x-ray transform. For RPD systems LORs suffer sensitivity loss with increasing perpendicular distance from the axis of rotation. Rotation factors ρ_i for each LOR i were used to incorporate this effect. For a given LOR with perpendicular distance y' from the axis of rotation, ρ_i is equal to the azimuthal angular range ϕ_R of rotation of the detectors for which the LOR is measurable (figure 1)

$$\phi_R(y') = 2\left[\arctan\left(\frac{L}{S}\right) - \arcsin\left(\frac{y'}{\sqrt{L^2/4 + S^2/4}}\right)\right]. \tag{6}$$

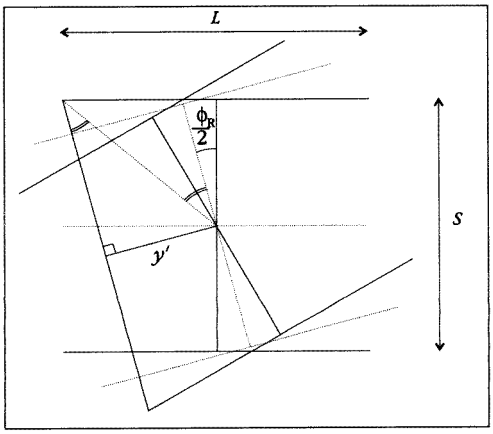

Figure 1. Geometry in transverse plane used for derivation of rotation factors for RPDs of length L and separation S.

3.2. EM–ML

For EM–ML the forward-projection algorithm used for the x-ray transform was projection-bin driven, calculating contributions at unit steps along each LOR using trilinear interpolation of the eight nearest voxels. Correspondingly the application of the transpose of the system matrix was implemented by the backprojection process, which was image-voxel driven, using bilinear interpolation of the projections to determine contributions. The rotation factors ρ_i were applied to the forward-projected values. The normalization matrix $\sum_i a_{ij}$ was found simply by the number of backprojection contributions.

3.3. FAIR

For FAIR the forward and backprojection used for the x-ray transform system model both had to be LOR driven, and so both used trilinear interpolation. The normalization matrix $\sum_i a_{ij} = w_j$ was derived analytically to account for all possible LORs. The rotation factors ρ_i were applied to the forward-projected values for each list-mode event. In principle any other data corrections needed (such as attenuation and scatter) can be applied in the same way. Equation (4) can now be rewritten as

$$f_j^{kN+n+1} = \frac{f_j^{kN+n}}{w_j} \sum_{i=\alpha_n}^{\beta_n} \left(\frac{1}{q_i^{kN+n}} \frac{a_{ij}}{\rho_i} \right). \tag{7}$$

The sensitivity factors w_j, for any voxel j in the field of view (FOV), are given by the total copolar angular range of the coincidence detectors seen by that point for a complete 180° rotation of the detectors. The required weight, w, for a given radial and axial position can be found by the integral

$$w(r, z) = \int_{-\pi/2}^{+\pi/2} \frac{1}{2\phi_R} \int_{-\phi_R}^{\phi_R} [\varepsilon(r, z, \eta, \phi) + \gamma(r, z, \eta, \phi)] \, \mathrm{d}\phi \, \mathrm{d}\eta \tag{8}$$

where the angles ε and γ (figure 2) are given by

$$\varepsilon(r, z, \eta, \phi) = \min \left[\arctan \left(\frac{W - 2z}{S' - 2r \cos \eta} \right), \arctan \left(\frac{W + 2z}{S' + 2r \cos \eta} \right) \right] \tag{9}$$

and

$$\gamma(r, z, \eta, \phi) = \min \left[\arctan \left(\frac{W + 2z}{S' - 2r \cos \eta} \right), \arctan \left(\frac{W - 2z}{S' + 2r \cos \eta} \right) \right] \tag{10}$$

with $S' = S / \cos \phi$. The integral over ϕ in (8) is used to obtain the mean length of S'. A discrete calculation of (8) was made for a series of radial and axial positions before interpolation into w_j.

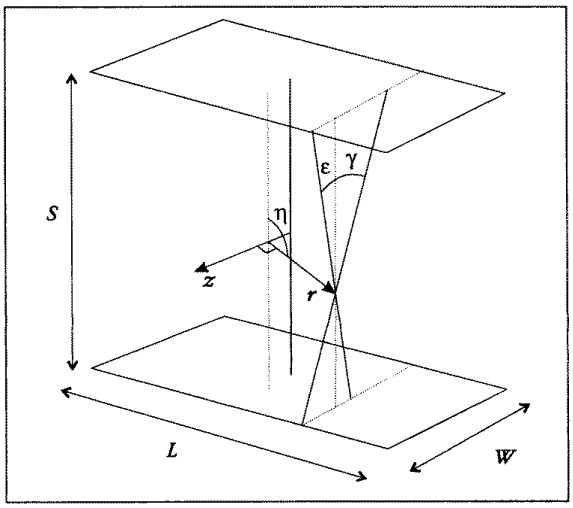

Figure 2. Geometry used for derivation of the axial sensitivity factors for RPDs of axial extent W.

4. Methods

The FAIR algorithm was compared with a standard implementation of the EM–ML algorithm in terms of resolution, noise, contrast and speed, using simulated data for an RPD geometry. The simulations included the effect of rotation but excluded the effects of attenuation and scatter. The geometry chosen (figures 1 and 2) was such that $W = 300$ mm, $L = 600$ mm and $S = 1100$ mm giving a maximum copolar angle of 15.25°, consistent with the dimensions of the current scanner at this hospital, MUP-PET (Marsden *et al* 1989).

4.1. Resolution

Two million events were simulated from six point sources located at six different positions in the FOV: (0, 0, 0), (53, 0, 0), (107, 0, 0), (0, 0, 107), (53, 0, 107) and (107, 0, 107) ((x, y, z) in mm). Reconstructions were made with one to eight iterations of FAIR and one to eight iterations of EM–ML. The images were reconstructed into a cylindrical volume 320 mm in diameter and length (within a 128^3 matrix) using cubic voxels of 2.5 mm side. The standard EM–ML reconstructions used 2D parallel projections of 128^2 elements with 96 azimuthal samples (1.875° sampling interval) and 7 copolar samples (4.357° sampling interval). The full width at half-maximum (FWHM) and at tenth-maximum (FWTM) (where the maximum was taken to be the maximum voxel value) for each of the six reconstructed point sources were evaluated radially, tangentially and axially using cubic spline interpolation, and mean values were then calculated.

4.2. Noise

Eight million coincidence events from a uniformly active cylindrical phantom were generated by Monte Carlo simulation. This number of events was chosen in order to assess FAIR over 64 iterations, using just *one* data subset, within a computationally feasible time. The diameter of the phantom was 200 mm, and the axial length 300 mm (equal to the axial FOV). Reconstructions were made with 1 to 64 iterations of FAIR using 1, 8, 16, 32 and 64 subsets of the list-mode data, and also with 1 to 64 iterations of EM–ML. The images were reconstructed into a cylindrical volume 300 mm in diameter and length (within a 64^3 matrix) using cubic voxels. The standard EM–ML reconstructions used 2D parallel projections of 64^2 elements with 96 azimuthal samples (1.875° sampling interval) and 7 copolar samples (4.357° sampling interval). The standard deviation in the whole reconstructed cylinder and in each transverse plane was calculated.

4.3. Contrast

Eight million events from a cylinder (of the same dimensions as in section 4.2) with hot and cold inserts of different sizes were simulated. The inserts were spheres with diameters of 2, 4, 6 and 8 voxels, centred in two different transverse planes 75 mm from the central transverse plane. The relative activity concentrations in the cold spheres, background and hot spheres were 0, 1 and 2 respectively. Reconstructions were carried out as described in section 4.2, and the contrast recovery coefficient (CRC) for each insert was calculated using $|B - S|/B$, where S is the number of counts in a region corresponding to the whole sphere and B is the number of counts in a two voxel thick spherical layer surrounding the sphere. The mean square error (MSE) in the phantom was also calculated.

4.4. Speed

The speed increase of FAIR over a conventional implementation of EM–ML was calculated as a function of events for three different copolar sampling intervals of the projections used for the standard EM–ML. The calculation was based simply on the number of LORs incorporated in each iteration.

5. Results

5.1. Resolution

Figure 3 shows the tangential, radial and axial FWHM for FAIR and EM–ML. Mean values of the six point sources are shown and the range from minimum to maximum FWHM is indicated by error bars. FAIR has consistently lower mean values than EM–ML and significantly lower variation around the mean value. At the centre of the FOV (where the best resolution is obtained for EM–ML) there is little difference between FAIR and EM–ML; however, towards the periphery of the FOV FAIR maintains consistently good resolution whilst the EM–ML resolution degrades. FAIR demonstrates consistent and equal resolution in all three of the tangential, radial and axial directions. For the axial resolution FAIR converges after the first iteration even though the data were not reduced into subsets. The same trends were observed for the FWTM values.

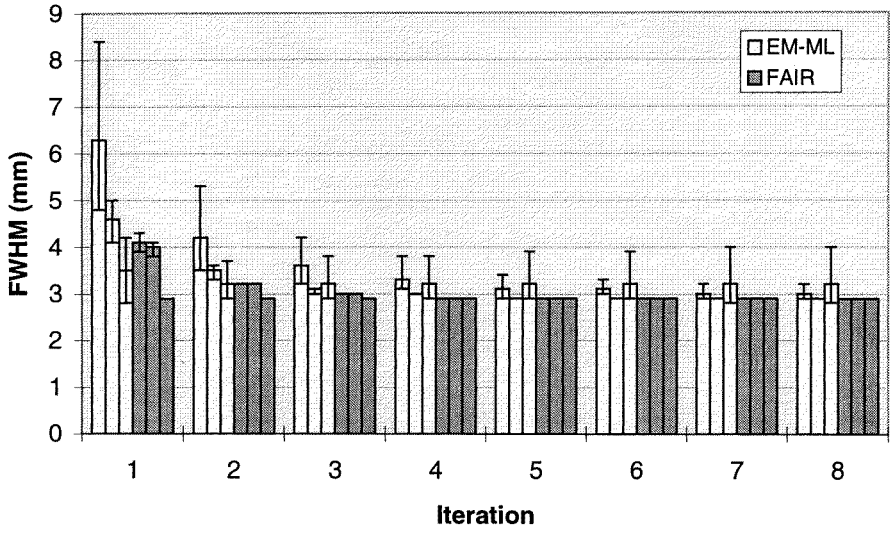

Figure 3. Tangential, radial and axial FWHM mean values for six point sources for FAIR and EM–ML. The bars correspond to tangential, radial and axial FWHM values respectively for each method for each iteration. The 'error' bars indicate the maximum and minimum FWHM values which always occurred at the largest radial locations and at the centre respectively.

5.2. Noise

Figure 4 shows the standard deviation (SD) in the whole of the uniform phantom reconstructed with FAIR for 1, 8, 16, 32 and 64 subsets and also with EM–ML as a function of iterations (or subiterations for FAIR). The SD for FAIR is consistently lower

than that for EM–ML. Initially the SD increases rapidly, then levels out between iterations 4 and 8, before starting to increase again monotonically. This behaviour is related to the axial SD distribution shown in figure 5. The SD for FAIR (figure 5(*a*)) and EM–ML (figure 5(*b*)) is shown as a function of axial position for 1, 2, 4, 8, 16 and 24 iterations. In the first four iterations the SD increases in all planes. Between iterations 5 and 8 the SD continues to increase in the edge planes, but decreases in the central ones. Beyond 16 iterations the SD increases in all planes. This effect is not present in 2D reconstructions and is clearly a result of redundant data. The SD curves for the FAIR reconstructions are more continuous and less erratic than the EM–ML SD curves which demonstrate discontinuities due to the discrete number of copolar angles of the binned projection data.

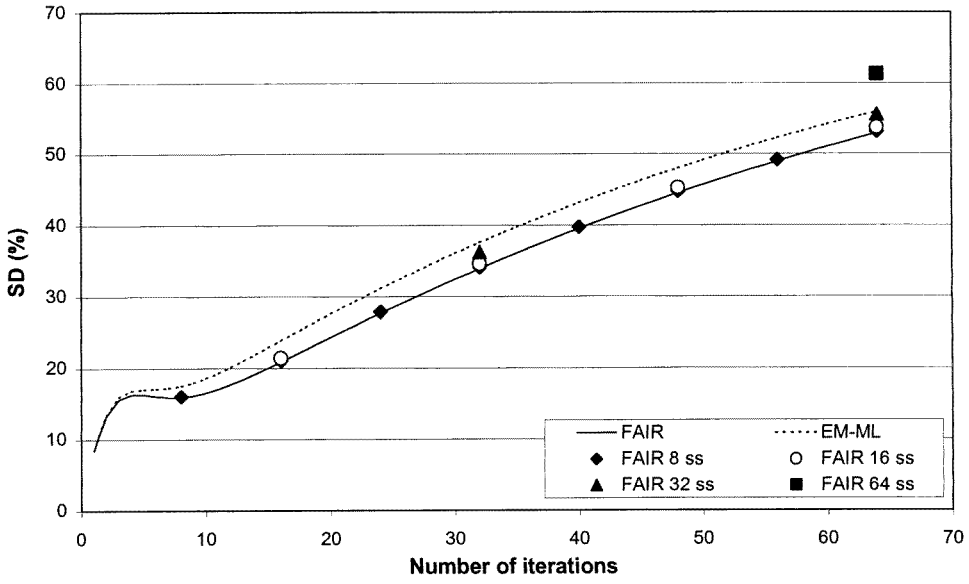

Figure 4. Standard deviation (SD) in the uniform phantom as a function of iterations/subiterations for FAIR with 1, 8, 16, 32 and 64 subsets and for EM–ML.

5.3. Contrast

The contrast of the smallest and largest inserts of the contrast phantom are shown as a function of iterations in figure 6(*a*) for hot and in figure 6(*b*) for cold inserts. As for the uniform cylinder, the results for FAIR using differing numbers of subsets are presented in addition to the comparative results between FAIR and EM–ML for one data subset. FAIR offers improved hot and cold contrast compared with EM–ML, the improvement being greater for the small spheres. For the cold inserts, the FAIR results obtained with a number of subsets greater than one follows the one-subset curve but, for the hot inserts, the results deviate slightly from the curve, the deviation increasing with increasing number of subsets.

The mean square error (MSE) in the contrast phantom is shown in figure 7 as a function of iterations for EM–ML and for FAIR with differing numbers of subsets. A minimum occurs after eight iterations, corresponding to the plateau region in the SD curve (figure 4). The eight-subset result for FAIR follows the one-subset curve closely but, with increasing subsets, the MSE increases beyond the values obtained using one subset.

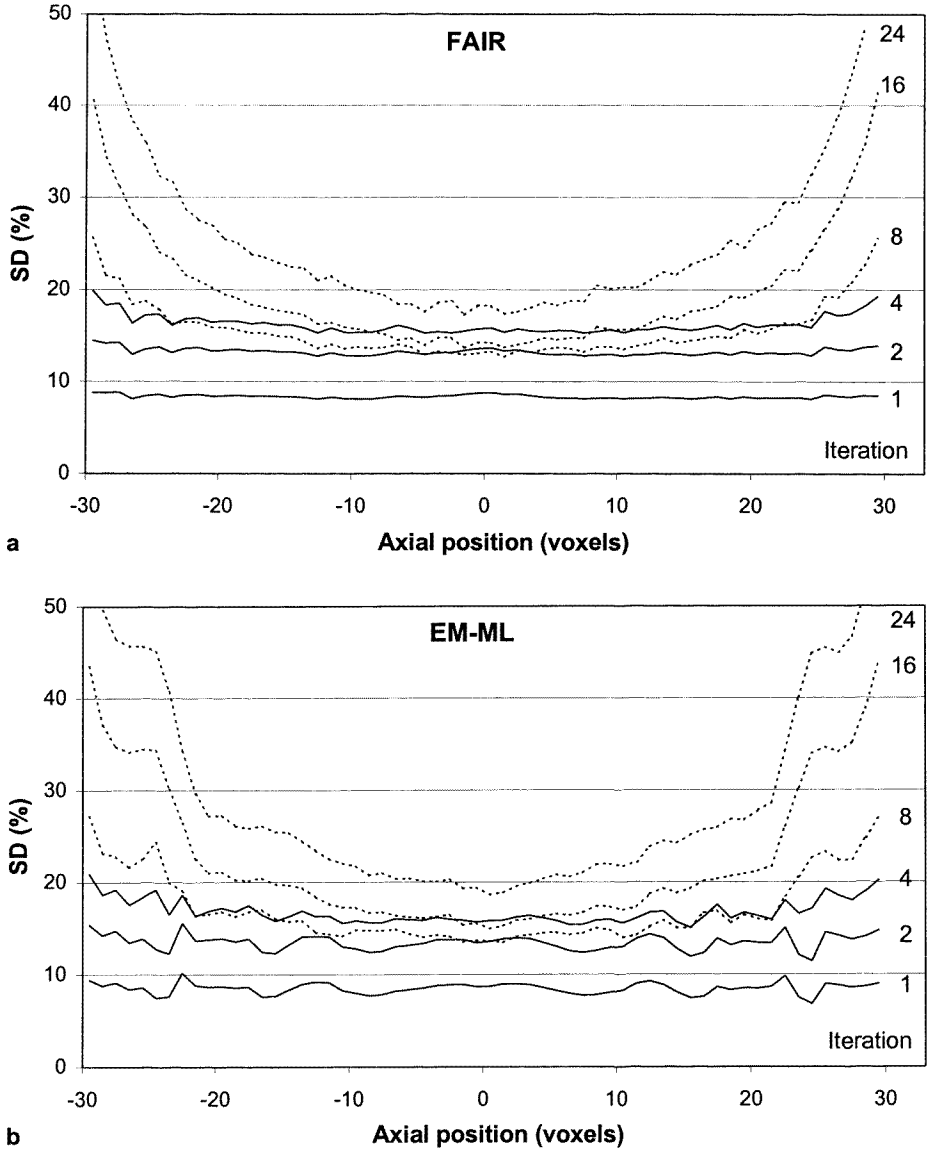

Figure 5. Axial distribution of standard deviation (SD) for (*a*) FAIR and (*b*) EM–ML with 1, 2, 4, 8, 16 and 24 iterations.

5.4. Speed

Figure 8 shows the speed increase of FAIR over standard EM–ML. These speed increase factors have only been calculated for one subset. The most substantial speed increases occur when there are fewer than five million events. The break-even point is where the number of LOR bins in the projection data used for the standard EM–ML match the number of events in the list-mode data used for FAIR. For higher statistical levels, where the number of list-mode events exceed the number of projection bins, FAIR actually reconstructs more slowly than standard EM–ML, but of course whilst maintaining its improved accuracy.

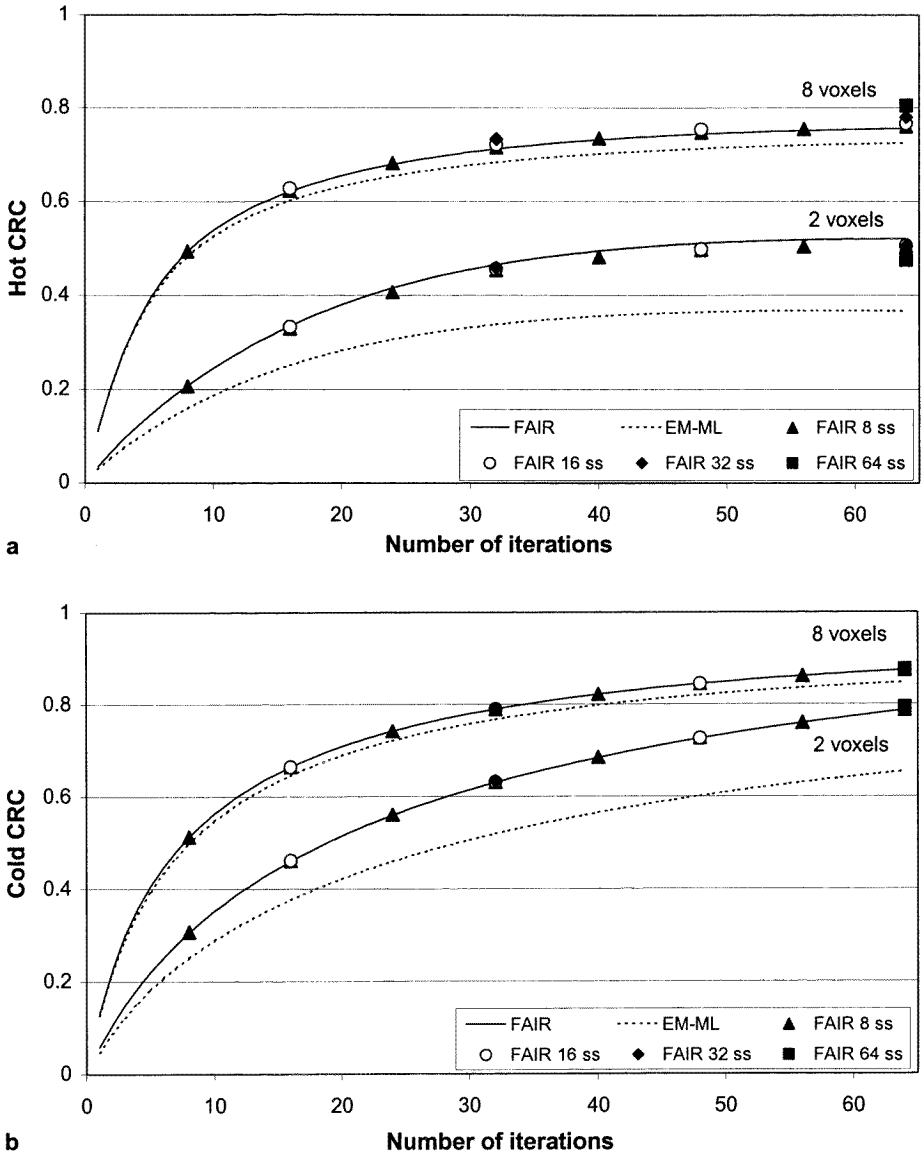

Figure 6. Contrast recovery coefficient (CRC) for the smallest and largest (*a*) hot inserts and (*b*) cold inserts of the contrast phantom as a function of iterations for FAIR with 1, 8, 16, 32 and 64 subsets and for EM–ML.

6. Discussion

The results show that FAIR can give images with improved spatial resolution, higher contrast and lower noise in less reconstruction time (for low statistics and/or through use of subsets) than a conventional implementation of the EM–ML algorithm for an RPD-based PVI scanner. This is due to complete utilization of the positional information contained in the list-mode data which is lost when histogrammed into coarsely sampled projections. The

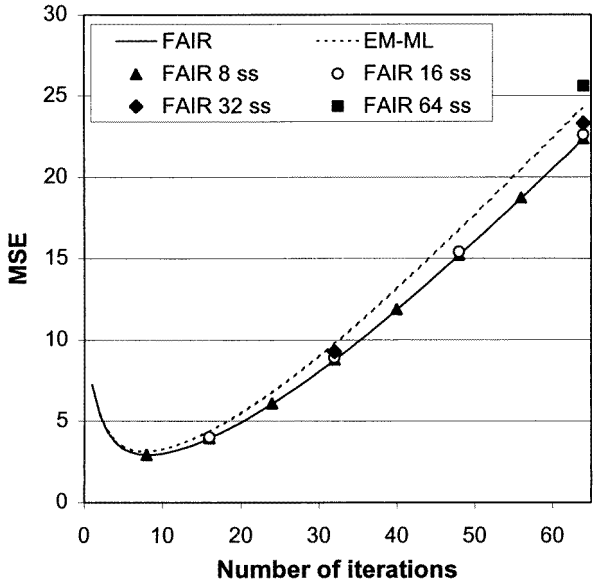

Figure 7. Mean square error (MSE) in the contrast phantom as a function of iterations for FAIR with 1, 8, 16, 32 and 64 subsets and for EM–ML.

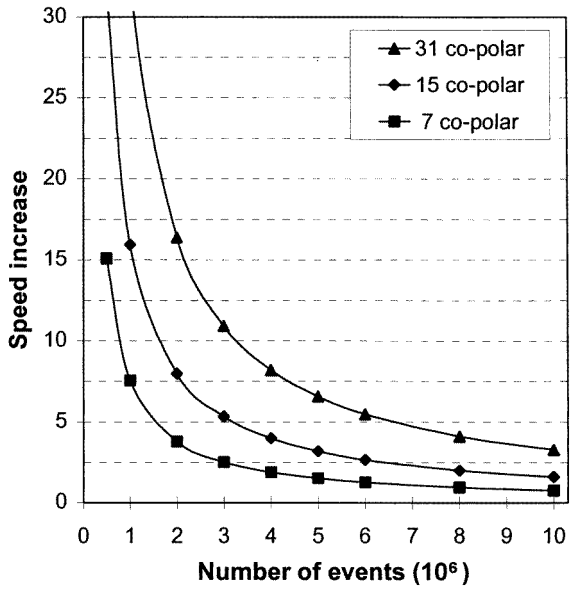

Figure 8. Speed increase as a function of number of events used when compared with standard EM–ML operating on 128^2 2D projections with 128 azimuthal samples and 7,15 or 31 copolar samples.

results indicate that the standard EM–ML method based on 2D parallel projections has a more erratic axial noise variation and poorer consistency in the axial and tangential resolution throughout the FOV due to the comparatively poor copolar and azimuthal sampling. Such

coarse sampling is inevitable, due to the dramatic increase in memory and computational requirements which occurs with improved sampling of the four-dimensional projection data set. For example, RPD-based systems such as MUP-PET allow 511 possible copolar angles to be measured, which is over an order of magnitude greater than that usually used in practice for projection data. In this case, a standard projection-data based implementation of EM–ML would be impractical if all the LOR sampling precision were to be retained.

Direct use of list-mode data for reconstruction removes systematic image reconstruction artefacts which are introduced by software rebinning. Thus with list-mode based reconstruction the accuracy limits are set by the detector hardware alone and not the software. These results found for RPD-based systems are also relevant to discrete-crystal detector-based systems with a large axial extent which inherently incorporate a large number of possible copolar angles. The results here suggest that reducing the number of azimuthal and/or copolar samples to reduce data set sizes, so-called 'mashing', should be avoided. As detector sampling intervals improve and FOV sizes increase so processing and storage of the fully accurate projection data becomes less viable, forcing a choice between list-mode storage or projection data sampled more coarsely than the hardware spatial sampling rate.

The FAIR algorithm can be accelerated by dividing the list-mode data into subsets and performing one reconstruction iteration for each subset, giving an acceleration factor equal to the number of subsets. The sequential time subsets of the list-mode data used here are unsorted, as opposed to the ordered subsets proposed for EM–ML (Hudson and Larkin 1994), and correspond to complete low-statistics tomographic data sets. The noise, contrast and MSE results obtained using eight subsets (1 million counts/subset) are essentially the same as with one subset, and with 16 subsets (0.5 million counts/subset) the difference is marginal. This indicates that, by using subsets with more than 0.5 million counts (for the detector geometry, activity distribution and matrix size used here), images are obtained with the same characteristics as those obtained with one subset, which converge to the ML solution. To allow more scope for varying the number of data subsets and hence the effective number of iterations achievable with one pass through the data, a modified version of FAIR could be used

$$f_j^{kN+n+1} = f_j^{kN+n} + \lambda^k f_j^{kN+n}\left(\frac{\sum_{i=\alpha_n}^{\beta_n}[(1/q_i^{kN+n})a_{ij}]}{\sum_{i=1}^{I} a_{ij}} - 1\right) \tag{11}$$

where λ^k is an over-relaxation parameter (Lewitt and Muehllehner 1986). In principle by using (10) and considering the number of events in the data set it should be possible to arrive at the required number of EM–ML equivalent iterations by just one pass through the list-mode data. Careful selection of λ^k would be necessary.

The FAIR algorithm is most applicable to scanners with high spatial sampling and to low-statistics imaging situations such as fast whole-body (WB) surveys and fast dynamic studies. For reconstruction of fast WB surveys carried out with continuous couch movement FAIR retains all axial sampling information and possibly offers data compression when compared with storing a series of projection data sets for a discrete number of couch positions. For multiple frame dynamic reconstructions FAIR can offer considerable acceleration due to the low-statistics nature of most dynamic acquisitions. Even for systems which physically bin data into tubes of response the FAIR approach still offers fast reconstructions through use of time-frame data subsets, offering the scope for real-time iterative reconstruction.

Acknowledgments

A J Reader was funded by the Medical Research Council and K Erlandsson by the European Union (grant #BMH4CT96023).

References

Barrett H H, White T and Parra L C 1997 List-mode likelihood *J. Opt. Soc. Am.* A **14** 2914–23

Browne J and De Pierro A R 1996 A row-action Alternative to the EM algorithm for maximising likelihoods in emission tomography *IEEE Trans. Med. Imaging* **15** 687–99

Hudson H M and Larkin R S 1994 Accelerated image reconstruction using ordered subsets of projection data *IEEE Trans. Med. Imaging* **13** 601–9

Lewitt R M and Muehllehner G 1986 Accelerated iterative reconstruction for positron emission tomography based on the EM algorithm for maximum likelihood estimation *IEEE Trans. Med. Imaging* **5** 16–22

Marsden P K, Ott R J, Bateman J E, Cherry S R, Flower M A and Webb S 1989 The performance of a multiwire proportional chamber positron camera for clinical use *Phys. Med. Biol.* **34** 1043–62

Parra L C and Barrett H H 1998 List-mode likelihood: EM algorithm and image quality estimation demonstrated on 2D PET *IEEE Trans. Med. Imaging* at press

Schmidlin P, Bellemann M E and Brix G 1997 Iterative reconstruction of PET images using a high-overrelaxation single-projection algorithm *Phys. Med. Biol.* **42** 569–82

Shepp L A and Vardi Y 1982 Maximum likelihood reconstruction for emission tomography *IEEE Trans. Med. Imaging* **1** 113–22

Tanaka E 1987 A fast reconstruction algorithm for stationary positron emission tomography based on a modified EM algorithm *IEEE Trans. Med. Imaging* **6** 98–105